# Influence of Electrostatic Interactions on Spin-Assembled Single-Walled Carbon Nanotube Networks on Amine-Functionalized Surfaces

**Justin P. Opatkiewicz, Melburne C. LeMieux, and Zhenan Bao***

Department of Chemical Engineering, Stanford University, Stanford, California 94305

**ABSTRACT** Preferential interactions between self-assembled monolayers (SAMs) terminated with amine functional groups and single-walled carbon nanotubes (SWNTs) were exploited to produce nanotube networks (SWNTnts) *via* spin coating. We provide insight into the mechanisms of this system while simultaneously demonstrating a facile approach toward controllable arrays of SWNTnts. The chirality, density, and alignment of the SWNTnt was heavily influenced by adsorption onto amine-functionalized surfaces that were exposed to varying pH solutions, as evidenced by atomic force microscopy (AFM) and Raman spectroscopy. This pH treatment altered the charge density on the surface, allowing for the examination of the contribution from electrostatic interaction to SWNT adsorption and SWNTnt characteristics. Secondary and tertiary amines with methyl substitutions were utilized to confirm that adsorption and chirality specific adsorption is largely due to the nitrogen lone pair, not the neighboring hydrogen atoms. Thus, the nature of adsorption is predominantly electrostatic and not due to van der Waals forces or localized polarization on the SWNTs. Moreover, the overall density of SWNTnts is different for the various amines, indicating that the accessibility to the lone pair electrons on the nitrogen plays a crucial role in SWNT adsorption. With greater understanding of the amine—SWNT interaction, these findings can be utilized to control SWNTnt formation for the precise integration into electronic devices.

**KEYWORDS:** self-assembled monolayer · electrostatic interactions · carbon nanotube network · nanotube adsorption

The need for highly durable materials with excellent electrical properties[1−3] has led to interest in carbon nanotubes (CNTs) as potential building blocks for bendable, large area electronics including applications such as flexible electronics,[4−6] sensors,[7−11] and photovoltaics.[12,13] However, this potential has yet to be realized due to fundamental problems that naturally arise in the synthesis and device fabrication processes. CNTs are produced in a mixture of semiconducting and metallic types during synthesis, impeding most electronic applications, especially CNT field effect transistors (CNT-FETs) where it is desirable to have only one or the other. Many separation or purification processes have been developed in recent years to solve this problem including density gradient ultracentrifugation,[14] selective side wall functionalization to suppress metallic conductivity,[15,16] electrical breakdown of metallic tubes,[17] polymer wrapping,[18] and many more.[19−23] Most of these techniques suffer from difficulty of scaling up, requiring electric or magnetic fields, or the requirement of having small molecules or surfactants wrapped around the tubes which can alter their electrical properties.

Another major roadblock is the directed assembly straight from solution of SWNTnts with tunable density and alignment into rational device layouts over large areas. Mats of chemical vapor deposition (CVD) grown networks for CNT-FETs have been shown by Snow *et al.* to produce high current densities with hole mobilities ranging from 10 to 100 $cm^2 V^{-1} s^{-1}$.[24] However, on/off ratios are typically low ($10^2$) in such films due to lack of chirality separation, unless the metallic tubes are burnt off[17] or additional etch lines are carved into the network to cut metallic percolation pathways.[25] Still, CVD is not compatible if desired applications include use of flexible substrates due to the high temperatures needed. However, microcontact transfer of CVD mats or printing of nanotube inks from PDMS stamps onto receiving substrates has potential in flexible electronics applications.[26]

On the other hand, network devices fabricated by solution deposition provide for a straightforward, one-step fabrication alternative and can, in principle, be utilized at a reasonable manufacturing scale,[27] while yielding similar electronic properties. Several groups have developed innovative approaches to achieve orientation control over large area solution-assembled SWNT films including microfluidics,[28] external

*Address correspondence to zbao@stanford.edu.

Received for review October 9, 2009 and accepted January 05, 2010.

**Published online January 29, 2010.**
10.1021/nn901388v

fields,[29] and flow/capillary alignment.[30] Another demonstrated practice includes the patterning of different hydrophilic/hydrophobic SAMs having attractive/repulsive interactions toward nanotubes to control the solution deposition of nanotubes into specific patterns.[31−33] None of these aforementioned methods separate semiconducting and metallic nanotubes to a suitable degree. Moreover, these are multistep processes that potentially limit device layout and provide minimal control over the density of SWNTs and degree of alignment, which also dramatically influences charge transport in the network.[34] Overall, lack of chirality sorting and alignment leads to significant numbers of Schottky barriers that arise at intertube junctions and hence increased resistances in CNT-FETs.[35] Thus, despite the great progress, these networks still suffer from low on/off current ratios. For these reasons, a means of depositing SWNTnts from solution while aligning and separating SWNTs by chirality is a highly desired technique for nanotube films in general to enable electronic and other applications.

We recently demonstrated such a technique, consisting of solution deposition of a SWNTnt onto functionalized surfaces to produce nanotube films with tunable properties that could be readily scaled to large area deposition.[36] In this process, substrates were modified by SAMs with a variety of organic functional groups. Nanotubes, deposited using a spin-assembly technique, interacted with and adsorbed onto the modified surface forming aligned networks. Different levels of interactions with the molecular functional groups on the SAMs led to varying levels of alignment, density, and enrichment of the semiconducting or metallic nanotubes. In the study, it was found that amine-functionalized surfaces adsorbed primarily semiconducting nanotubes (sc-SWNTs), while aromatic surfaces adsorbed primarily metallic (met-SWNT) networks.

Whereas the interaction between aromatics and met-SWNTs has been thoroughly investigated theoretically,[37−39] the origin of the interaction and influence of amines with SWNTs is less understood. Early studies had shown that bulk nanotube solutions could be enriched with sc-SWNTs by mixing with aminated molecules and precipitating out met-SWNTs.[21] Some groups have reported that the lone pair electrons on the nitrogen noncovalently bind to the nanotube side wall, donating electron density and producing relatively strong physisorption binding energies.[40−42] In the latter work, it was found that the local polarization on the SWNTs from the amine was strong enough to significantly alter the electrical conductivity of the sc-SWNTs. Others have carried out single molecule experiments and simulations suggesting a hydrogen atom on the nitrogen, not the lone pair, orients toward the nanotube wall and the interaction can be dispersive in nature.[43,44]

These possible modes represent a wide discrepancy in interaction energies, and one could envision this resulting in a wide range of CNT adsorption that can be precisely controlled if understood better. Previous research mainly demonstrated that CNTs can be adsorbed on this SAM. For such a potentially critical system in the rational design of nanomaterials, the adsorption of SWNTs onto such surfaces with precise location and density has only been studied on a relatively limited basis. The majority of this work has dealt with bath adsorption (long soaking times) of both functionalized and nonfunctionalized tubes from solution onto hydrophilic or hydrophobic/hydrophilic surface patterns; however, it is anticipated that, for device applications, SWNT films will be assembled by more dynamic processes.

Burgin *et al.* examined the electrostatic nature of nanotube adsorption on amine surfaces where both the amine and the SWNTs were treated to various pH buffers prior to bath deposition of nanotubes.[45] The study was complicated by potential partial coverage or multilayers in the amine SAM (partially exposing the amine, oxide, silane headgroup, or a combination of these on the surface), making it difficult to conclude the interaction mechanism for SWNT adsorption. This is alleviated by fabricating a true amine monolayer, which is not a trivial process. Also the deposition technique of immersing substrates in a CNT solution for a long time span yielded a thick multilayer network of SWNTs on the surface. Beyond the first layer of amine−CNT interaction, the additional CNTs can be simply adsorbed onto the nascent layer through strong van der Waals forces, limiting the conclusions that could be drawn. It is also likely that the long deposition times of bath deposition will not allow for preferential interaction of amines with sc-SWNTs, critical for electronic applications. Recent work by the Strano group has nicely shown that functionalized SWNT adsorption depends on amine concentration reaching an optimal value at an intermediate concentration.[46] However, a relatively small gradient in amine concentration was used, and the tubes were intentionally functionalized with −COOH or −OH groups and deposited through bath adsorption. To date, no clear systematic mechanism has been revealed that could lead to a roadmap of precisely assembling SWNT films from solution for device applications.

In this work, the effect of electrostatic interaction between amine/SWNT during a more dynamic process (spin assembly) is investigated. The amine-functionalized surfaces were exposed to solutions of varying pH, and then nanotubes were immediately spin-cast on them. Because the ultimate goal of our research is to use these deposited SWNTs for electronic devices, the SWNTs were not intentionally functionalized nor was the solution treated with any pH solution, leaving the SWNT charge states unaltered, in contrast to the previous studies. Varying the pH allows for a tunable level of surface charges and hence a scalable approach to fine-tune SWNT network film formation. The

**TABLE 1. Influence of pH Treatment on APTES Monolayer Properties[a]**

| silane | untreated | pH 3 | pH 5 | pH 7 | pH 8 | pH 10 | pH 11 | pH 12 | pH 13 |
|---|---|---|---|---|---|---|---|---|---|
| CA (°) | 62.3 ± 1.1 | −1.9 ± 3.4 | −0.7 ± 1.2 | −2.2 ± 1.6 | −1.3 ± 1.0 | −1.5 ± 2.4 | −4.0 ± 1.1 | −6.6 ± 1.4 | −24.3 ± 2.9 |
| SWE (Å) | 6.3 ± 0.4 | −0.1 ± 0.9 | −0.9 ± 1.0 | −0.7 ± 0.8 | −0.8 ± 0.3 | −0.9 ± 0.4 | −1.8 ± 0.3 | −3.7 ± 0.3 | −5.7 ± 0.3 |
| $NH_3^+$ density (theory, $cm^{-2}$) | none | $3 \times 10^{11}$ | $3 \times 10^{9}$ | $3 \times 10^{7}$ | $3 \times 10^{6}$ | $3 \times 10^{4}$ | N/A | N/A | N/A |

[a]Contact angle (CA) and thickness measured by single wavelength ellipsometry (SWE) of primary amine (APTES) before exposure to various pH solutions (column 1). Subsequent columns identify the net change in contact angle or thickness after the pH treatment. The theoretical ammonium density is taken assuming the mean molecular area per APTES molecule is 30 $Å^2$, yielding an amine surface density of approximately $3 \times 10^{14}$ amine/$cm^2$. At pH 11 and beyond, the surfaces were physically altered, drastically reducing the number of amines present on the surface and turning off SWNT adsorption. In this case, the exact amine density is unknown, so proposed ammonium densities are not provided. Secondary (51 ± 1.5° CA, 5.4 ± 0.7 Å) and tertiary (45 ± 1.3° CA, 5.3 ± 0.7 Å) amines followed similar trends.

adsorption density, network alignment, and extent of chirality sorting were examined to determine which factors enhance or reduce the electrostatic attraction between the surface and the nanotubes and why. In addition, we examined three amine surfaces (primary, secondary, and tertiary amines) that are expected to have different levels of steric hindrance with regards to the electrostatic interaction with the nitrogen, and the influence of the amine hydrogen atoms on the adsorption was studied. With our systematic study, this work aims to give fundamental insight into SWNT interactions by revealing that varying surface protonation and adsorption energy can be utilized as a design parameter to precisely control the quality of the sc-SWNT network.

## RESULTS AND DISCUSSION

**Effects of Surface Protonation on CNT Adsorption.** Silicon substrates with native oxide were modified with 3-aminopropyltriethoxysilane (APTES) at room temperature in a nitrogen environment to form the amine-terminated SAM and analyzed with AFM, contact angle, and ellipsometry for film quality. To enable this study, a critical step is the fabrication of a clean monolayer of APTES on the surface. Contact angle averaged around 60°, similar to previously reported values on APTES monolayers, and did not degrade after exposure to water, indicating covalent grafting of the SAM. Typical film thicknesses and sample contact angles are listed in Table 1, showing APTES thickness around 6.3 Å (rms roughness <0.3 nm as determined by AFM), which is close to the theoretical thickness of about 7 Å and corresponds to a surface density of around $3.4 \times 10^{14}$ $NH_2$/$cm^2$.

After SAM modification, the samples were placed in individual vials containing HCl or NaOH solution diluted to each desired pH, ranging from 3 to 13. This produced ammonium-coated surfaces with densities ranging from roughly $3 \times 10^{11}$ (pH 3) to less than $3 \times 10^4$ $NH_3^+$/$cm^2$ (pH 10 and higher). Upon removal from the pH bath, arc-discharged SWNTs dispersed in *N*-methylpyrrolidone (NMP) were spun-cast on each substrate at 4000 rpm. Previous work demonstrated that this spin rate yielded SWNTnts with high SWNT density, moderate alignment, and excellent thin film transistor (TFT) characteristics.[36] The AFM height images of the resulting SWNTnts are displayed in Figure 1, with the corresponding CNT densities and alignment data summarized in Table 2. The particles found on the pH 3 and 13 samples were a result of the unpurified HCl and NaOH being in high concentration and leaving particulates on the surface.

Overall, as the pH of the surface was increased from 3 to 13, the density of unmodified CNTs adsorbed on the surface was gradually reduced until approximately pH 12, where at pH 13 the number of tubes adsorbed

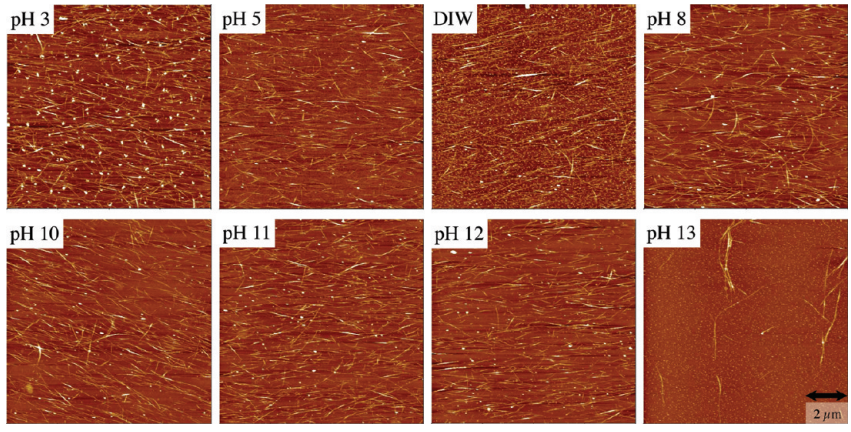


**Figure 1. AFM topography images of SWNTnts on APTES surfaces treated with different pH. With increasing pH, there is a general trend of reduced SWNT density and better alignment. Particles on the surfaces (especially on the pH 3 sample) were a result of impurities in the pH solutions. Note the elimination of a percolating network at pH 13. *Z*-scale ranges from 0 to 20 nm.**

**TABLE 2. Statistics of NT Adsorption on pH-Treated APTES**

| | pH 3 | pH 5 | pH 7 | pH 8 | pH 10 | pH 11 | pH 12 | pH 13 |
|---|---|---|---|---|---|---|---|---|
| SWNT density ($\mu m^{-2}$) | 20.8 ± 2.4 | 16.4 ± 3.6 | 17.3 ± 1.4 | 17.4 ± 1.3 | 12.8 ± 1.7 | 12.8 ± 1.5 | 11.4 ± 1.8 | 0.3 ± 0.02 |
| alignment SD (°) | 41.5 ± 8.2 | 31.5 ± 5.8 | 33.6 ± 6.2 | 29.7 ± 4.1 | 26.0 ± 2.8 | 20.9 ± 2.3 | 23.0 ± 1.1 | |

dropped drastically to almost 0 (per $\mu m^2$), as revealed by large-scale AFM images (Figures 1 and 2). We theorize that, as the APTES was treated with an aqueous environment at low pH, the amine functional groups convert to cationic ammonium ions. These positive ions likely interacted with the negatively charged carboxylate defect groups on the CNTs in solution. NMP used as a SWNT dispersion solvent serves as an effective proton acceptor due to its Lewis basicity.[47] Consequently, the CNTs containing negatively charged carboxylate defects can be attracted or repelled by a positively charged surface. Additionally, larger diameter nanotubes are likely to have more defects and hence be more charged and attracted to the surface. For arc-discharged SWNTs, larger diameter tubes are typically sc-SWNTs.

At very acidic pHs, the majority of the amines on the surface become positively charged. There was a strong electrostatic attraction between this surface and the negatively charged CNTs, leading to high density SWNTnts on the surface. As the pH increased, the number of ammonium ions decreased (see Table 1), weakening the electrostatic attraction of the CNTs to the surface. The density of CNTs gradually decreased from 21 SWNTs/$\mu m^2$ at pH 3 to nearly 50% of this value (12 SWNTs/$\mu m^2$) at pH 10, with this reduction in protonation confirming our claims of weakening interactions. The decrease in SWNT density was clearly evident until very high pH, near 13 (Figure 1). At this point, the SAM was partially etched away as evidenced by the ellipsometry and contact angle data in Table 1, and the CNTs were essentially in contact with bare oxide having very low amine coverage. There is minimal interaction/attraction between bare silicon oxide and SWNTs, leading to no adsorption. This overall trend is illustrated in Scheme 1.

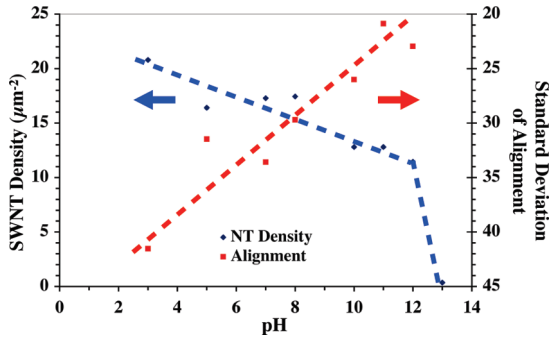


**Figure 2. SWNT adsorption and alignment as a function of bulk solution pH on APTES surfaces. The nanotube density and standard deviation of alignment about the average tube direction both gradually decrease with increasing pH of the bulk solution. Adsorption is effectively shut off beyond pH 12. Alignment data are not shown for pH 13 because the few nanotubes evident are random and show no alignment. Dashed lines serve as guiding lines.**

**Surface Protonation Effects on SWNT Alignment.** Coupled with the decrease in CNT density, a general increase in alignment could be observed as the pH was increased, as shown in Table 2 and Figure 2. AFM images were taken at roughly the same location on each sample for accurate comparison (see Figure SI-1 in Supporting Information). The most likely source of this trend is a result of the strength of the electrostatic and dispersive attraction between the surface and the nanotubes, here referred to as a physisorption energy. The radially flowing fluid serves as the aligning media for the system. If the attraction between the surface and the nanotubes is extremely high, as occurs at pH 3, the nanotubes will be strongly and essentially permanently bound to the surface (with a positive charge density of over $3 \times 10^{11}$/$cm^2$) and the fluid has no impact on dramatically altering tube alignment. Hence, the nanotubes deposited on this highly charged surface were less aligned, and the limited level of alignment observed was a result of the tubes being partially aligned while still in solution.

With increasing pH, the physisorption energy is reduced and the nanotubes are, at least momentarily, less strongly bound to the surface. In this situation, the nanotubes can touch down on the surface and be weakly bound to the surface initially. This allows the nanotube to be better aligned with the fluid flow prior to completely falling to the surface. After the entire length of the tube is in contact with the surface, they are then effectively bound by strong van der Waals forces. The random tubes deposited on the pH 13 surface are a result of residual fluid drying on the surface after spinning was stopped, and no alignment is observed in these cases. The fact that the alignment can be tuned is important for nanoelectronic devices and nanoscale sensors in which performance is directly affected by SWNTnt topology.[48,49]

**Raman Analysis.** In addition to demonstrating precise control over density and alignment, we aimed to see if the charges on the surface and subsequent SWNT/surface interaction had any affect on the types of SWNTs adsorbing. To determine the influence of the pH treatment on the surface-sorting abilities of APTES, micro-Raman analysis was used. Large areas across multiple samples were mapped using three excitation energies (2.33, 1.96, and 1.58 eV). The observed resonant radial breathing modes (RBMs) were then correlated to diameter and chirality by use of a Kataura plot and a RBM−diameter relationship determined by Dressel-

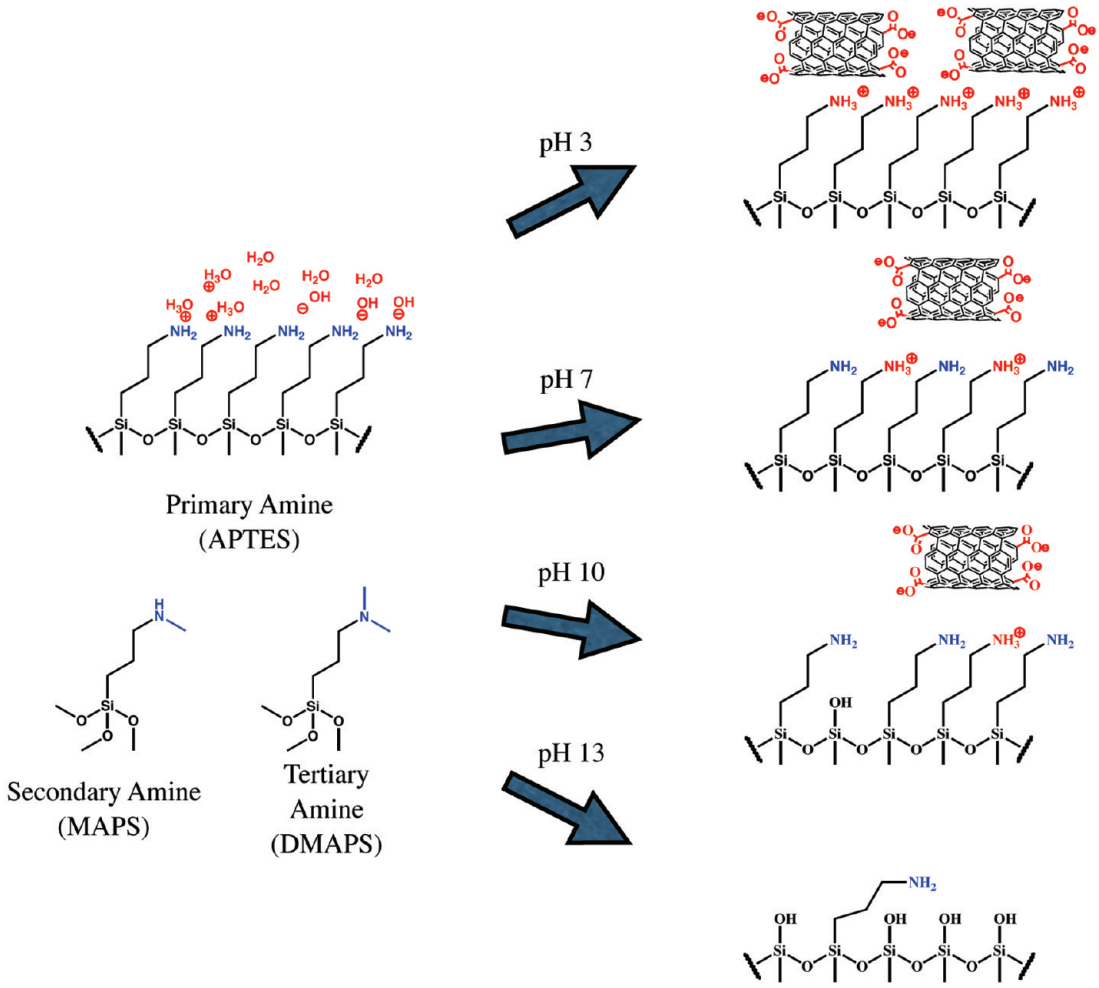


**Scheme 1. Influence of protonation on SWNT adsorption. Protonation of amines followed by SWNT adsorption. High densities of highly defective SWNTs adsorb to highly protonated surfaces. The density of the network reduces as the amines become less protonated. After treated with high pH solution, the surface is not attractive to SWNTs, and adsorption is shut off due to destruction of the SAM. The amine structures include primary (3-aminopropyltriethoxysilane, APTES), secondary (*N*-methylaminopropyltrimethoxysilane, MAPS), and tertiary (*N*,*N*-dimethylaminopropyltrimethoxysilane, DMAPS) substitutions.**

haus *et al.*[50,51] The RBM region of the compiled spectra is displayed in Figure 3. All spectra were normalized to the most common or intense peak in the RBM region (190, 172, and 160 $cm^{-1}$ for the respective excitations).

The 1.96 eV excitation is resonant with a nearly 50/50 mixture of metallic and semiconducting tubes and best demonstrates if the networks are being enriched in specific chiralities. All spectra in Figure 3a contain the peak at 172 $cm^{-1}$, corresponding to the average diameter of the nanotubes in the bulk solution. The higher energy shoulder corresponds to the $E^{M}_{11}$ transition of metallic tubes. The raw, unsorted network exhibits two metallic peaks (186 and 196 $cm^{-1}$) and has a broad metallic shoulder, which is partially suppressed in the SWNTnts on APTES surfaces, indicating that indeed there is a chirality selection occurring. Subtle differences arise between the spectra, particularly for surfaces treated with the lowest pH solutions, and there appears to be a high level of chirality sorting at higher pH. Whereas the pH 7−12 surfaces show roughly equal suppression of the 186 and 196 $cm^{-1}$ peaks, non-negligible enhancement of these peaks is observed at pH 3 and 5 relative to the higher pHs. The enhanced electrostatic attraction at low pH is very strong, and most nanotubes adsorb to the surface with minimal sorting taking place. Although the met-SWNTs should be less negatively charged than the sc-SWNTs (due to less carboxylate defects on the side walls), the surface charge density of $NH_3^+$ still appears large enough to attract them to the surface. For other surface treatments of pH greater than 5, this attraction was weaker. The met-SWNTs had weaker binding to these less densely protonated surfaces and could not overcome the strong shearing force in the spin assembly that removes the SWNTs from the surface. In contrast, the electrostatic attraction between the more defective and hence more charged sc-SWNTs could overcome the shear and adsorb to the surface.

The 2.33 and 1.58 eV excitations provide additional information with regards to the sorting on the surface.

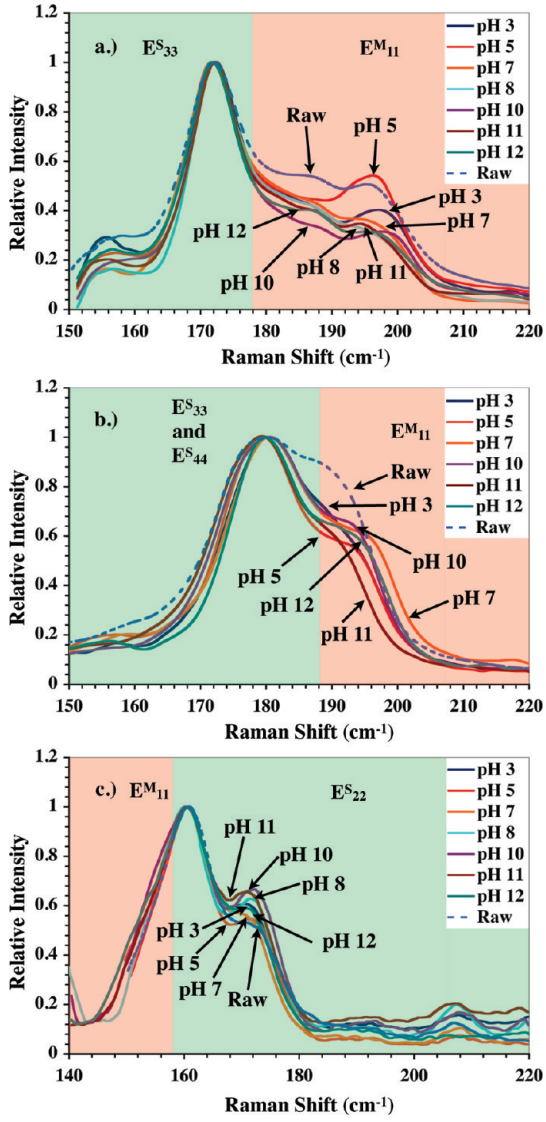


**Figure 3. Resonant Raman RBM analysis of NT networks on pH-treated amine surfaces at excitation energies of (a) 1.96 eV, (b) 2.33 eV, and (c) 1.58 eV.**

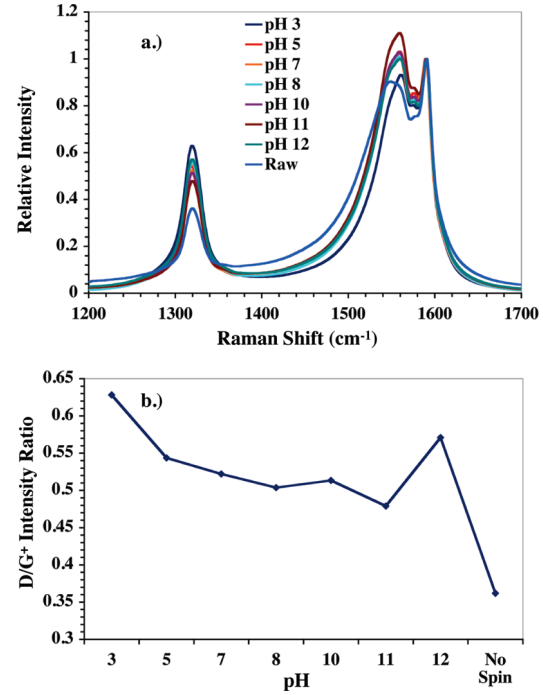


**Figure 4. D and G band analysis. (a) Raman spectra of 1.96 eV excitation of D and G band regions displayed. All spectra normalized to 1592 $cm^{-1}$ $G^{+}$ band. (b) Ratio of D/G band intensity as a function of pH. Decreasing trend corresponds to lower density of highly defective SWNTs adsorbed to the surface. The sudden jump in the D/G ratio at pH 12 is a consequence of more curved (more defective) SWNTs on the surface. The untreated, unsorted solution (labeled No Spin) shows no enhancement of defective tubes and a low D/G ratio. The "Raw" clearly has most G broadening since no separation takes place.**

At 2.33 eV, the SWNTnts yielded predominantly sc-SWNTs resonant with the $E^{S}_{33}$ and $E^{S}_{44}$ transitions and met-SWNTs resonant with the $E^{M}_{11}$ transition. Whereas the raw network showed relatively high adsorption of metallic tubes with resonant RBMs near 190 $cm^{-1}$, most pH-treated surfaces yielded suppression of this metallic peak to roughly equal degree. The lack in trend, in contrast to the 1.96 eV, is expected because these tubes likely have fewer defects (since they correspond to smaller diameters) and hence are less sensitive to pH alteration. For the 1.58 eV excitations, $E^{M}_{11}$ transitions were too weak to be isolated from the background so only semiconducting $E^{S}_{22}$ transitions were analyzed. With increasing pH, the 171 peak became slightly more pronounced indicating enrichment of sc-SWNTs, matching the findings of the 1.96 eV excitation.

Line shape analysis of the G bands (tangential shearing phonon modes) yielded limited information due to moderate densities of metallic tubes on all surfaces broadening the G band for all samples. Looking at the disorder-induced D band structure at approximately 1320 $cm^{-1}$ (at the 1.96 eV excitation), as the pH of the treated surface was increased, the intensity of the D band, relative to the $G^{+}$ band, steadily decreased, as shown in Figure 4a. The most defective tubes had a greater negative charge and hence were more strongly attracted to the surfaces with a significant density of ammonium ions—specifically the pH 3 surface. Nanotubes with high levels of defect densities lose their long-range conjugation and fall out of electronic resonance with the excitation wavelength. This results in the dampening of the tangential shearing mode peak intensities along with the enhancement of the defect band. The opposite effect occurs as the defect density is reduced. As the level of protonation was reduced on the surface, fewer defective SWNTs adsorbed, resulting in decreasing D band intensity and the D/G ratio, as displayed in Figure 4b. More defective tubes were present on surfaces exposed to the pH 12 conditions because the partially etched APTES layer attracted more curved (and defective) tubes. This has very important implications for SWNT-based transistors, as well as more wide ranging implications such as controlling SWNT defects for advanced nanoelectronics.

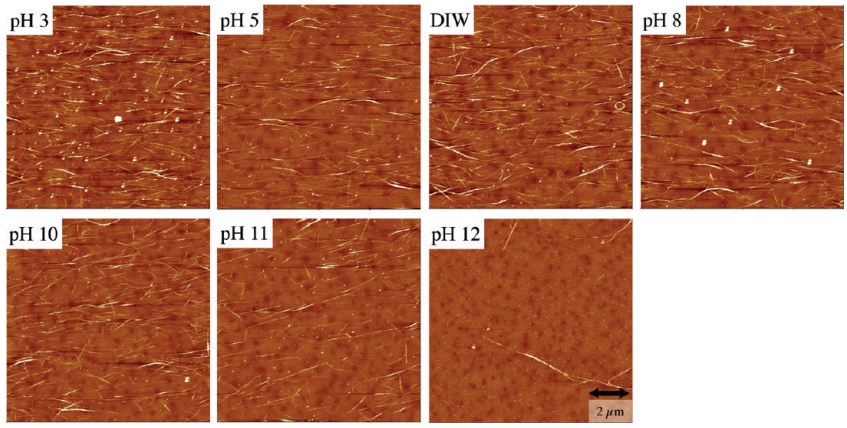


**Figure 5. AFM topography images of SWNTnts on secondary amine surfaces after pH treatment and NT deposition. Density and alignment trends mimic the primary amine surface. Pitting was present on the substrates prior to surface modification due to defective wafers. *Z*-scale ranges from 0 to 20 nm.**

**Altering Methyl Substitution.** To further elucidate the nature of the surface−SWNT interaction, we repeated the above experiments using the secondary (MAPS) and tertiary (DMAPS) amine surfaces (Scheme 1). This was used to understand if the steric hindrance of the donating group had any effect in this interaction. We also aimed to determine if the surface−SWNT interaction is primarily between the hydrogen on the amine or the ammonium cation as some simulation results indicated potentially stronger interactions with the hydrogen.[43] In contrast, work by Zhao *et al.* had suggested that, in the gas phase, methyl functional groups could have stronger interactions with SWNTs than amine groups.[52]

The AFM topographical images are shown in Figures 5 and 6. Immediately, we can observe that the density is much lower on these surfaces for a given pH relative to the APTES. The steric hindrance from the methyl groups during the surface modification led to lower density SAMs. The lower density of amines resulted in the surface ultimately having a lower density of ammonium ions for a given pH. Furthermore, the methyl groups sterically hindered the nanotubes from interacting with the amine lone pair. This methyl group "buffer" further weakened the electrostatic attraction between the surface and nanotubes. Hence lower SWNTnt densities were obtained overall, and nanotubes stopped adsorbing at lower bulk pH values.

Both surfaces yielded the same pH dependence trends of density and alignment as observed on the APTES surface. Increasing methyl substitution led to decreasing values of pH where CNT adsorption shutoff takes place. This trend is illustrated in the adsorption curves in Figure 7. Interestingly, the tertiary silane has nearly the same trend line as the APTES regarding decrease in SWNT *versus* pH. However, the secondary silane is relatively insensitive to pH changes until shutoff. Importantly, there are no studies carried out on characterizing the surface properties of these silanes, thus the configuration of the functional end group is not known. However, on the basis of CA measurements where the secondary amine was always consistently higher, we submit that the methyl group of the secondary amine may be more exposed to the surface, thus limiting this pH response sensitivity. On the other hand, the amine on the tertiary silane is more sterically hindered and less able to interact with the SWNTs, as the magnitude of SWNT adsorption is the lowest with this system (Figure 7). Similar to the APTES monolayers,

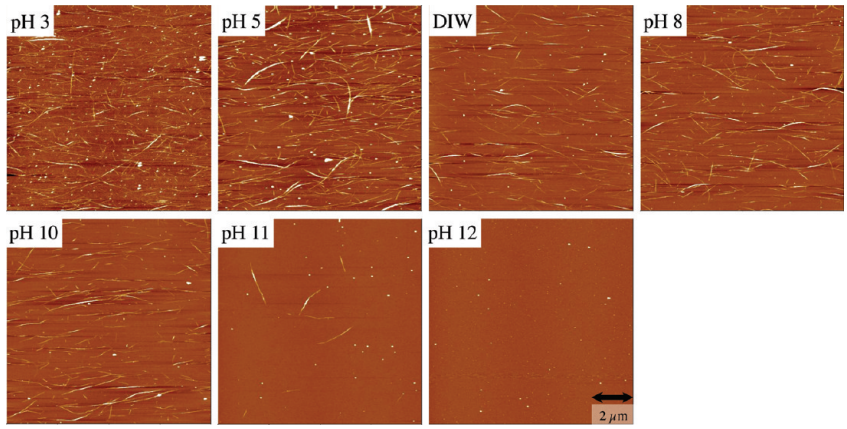


**Figure 6. AFM topography images of SWNTnts on tertiary amine surfaces after pH treatment, similar to Figures 2 and 5. Note the shutoff of SWNT adsorption takes place at far lower bulk solution pH values as compared to the primary amine. *Z*-scale ranges from 0 to 20 nm.**

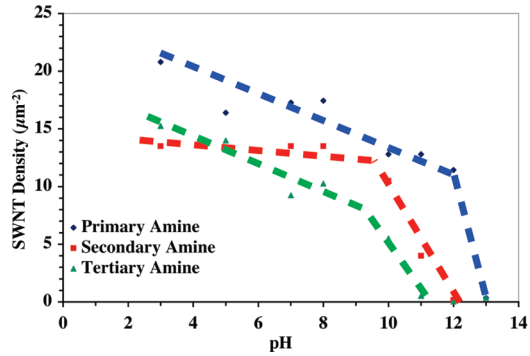


**Figure 7. SWNT adsorption as a function of bulk solution pH on all three amine surfaces. The nanotube density gradually decreased with increasing pH for all surfaces. Adsorption shutoff took place at decreasing pH as methyl substitution increased. The increased steric hindrance reduced the electrostatic interaction between the SWNTs and the amine, resulting in lower pH values producing adsorption shutoff.**

these surfaces experienced minor etching from pH 10 to 12 treatments but were still mostly intact. Therefore, shutoff was not a result of the complete removal of the monolayer.

The secondary and tertiary amine had a respectively weaker chirality sorting ability as compared to their primary amine counterpart. Enhancement of the $E^{S}_{33}$ transitions was evident with decreasing amine protonation for the 1.96 eV excitation on the secondary amine surface; however, virtually no trend was observed on the tertiary amine (Figure 8). No significant trend in the $D/G^{+}$ ratio confirmed minimal influence of amine protonation on these surfaces. The complete lack of any trend on the tertiary amine surface is likely a result of the steric hindrance caused by the methyl moieties. The 2.33 and 1.58 eV excitations, in contrast to the primary amine, showed no trends in chirality sorting on the secondary and tertiary amine surfaces and hence are not presented in this work.

As noted in the introduction, different interaction mechanisms have been discussed in the literature stating that the nanotube interaction with amines is *via* the hydrogen atoms on the amine, not the lone pair, and *vice versa*. While it has been demonstrated in single molecule measurements that the local polarization of the SWNT may occur under particular experimental conditions, it apparently does not apply in this more dynamic system. Our observation here of deposition of nanotubes on the secondary and tertiary amine surfaces seems to verify this theory. With or without the pH treatment, we observed nanotubes were adsorbed, even when no amine hydrogen atoms were present for interaction. Although the hydrogen atom may play some role, this work suggests that the lone pair is the dominant source of interaction and hence the source of chirality sorting when under a shearing flow. In addition to these fundamental insights, we have demonstrated that the secondary and tertiary amines can be

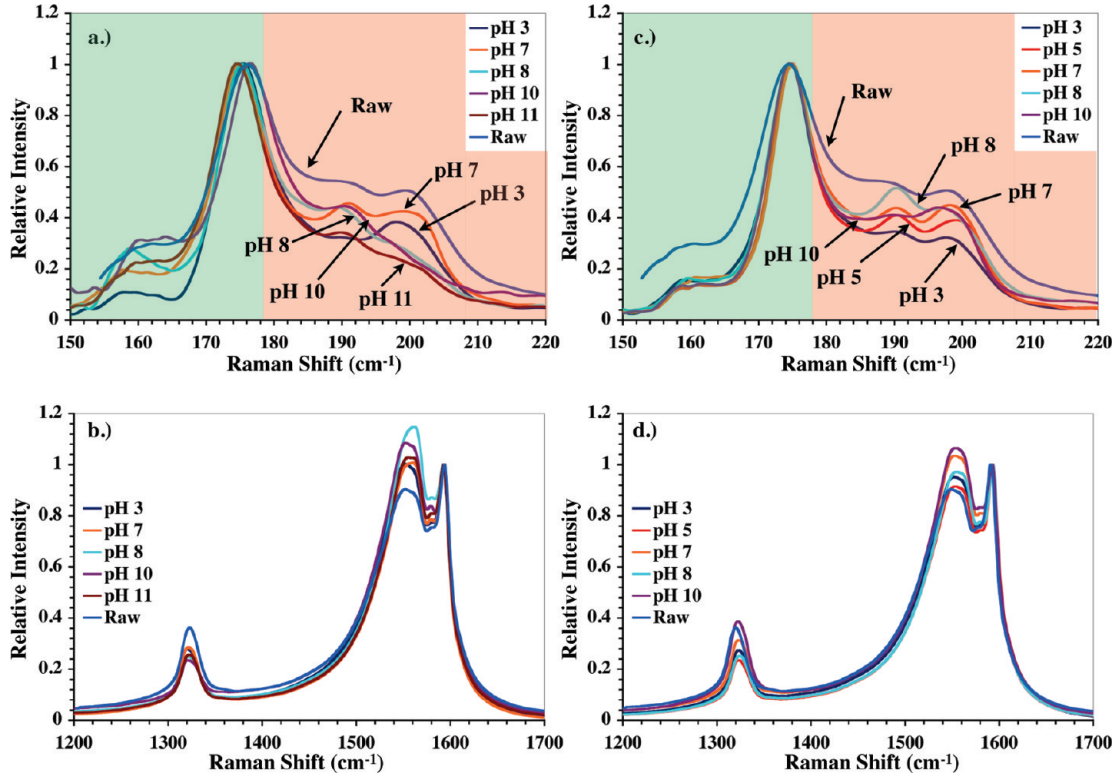


**Figure 8. Raman spectra of SWNTs on secondary and tertiary amines at 1.96 eV excitation. RBMs (a) and G bands (b) on the secondary amine (MAPS) surface. Corresponding spectra (c,d) on the tertiary amine (DMAPS) surface. Note, for the secondary amine, pH 11 yielded the best separation (weakest intensity of metallic peaks), whereas minimal trend was observed on the tertiary amine surface. Again, the "Raw" clearly has most G broadening since no separation takes place.**

used to further tune the level of adsorption and density in SWNTnts.

## CONCLUSIONS

In summary, we have fabricated amine silane SAMs with varying end groups that led to adsorption of submonolayer nanotube network films with varying degrees of alignment and density. The protonation of amine-coated surfaces influences this adsorption and chirality sorting of SWNTs. Protonated surfaces attract large densities of nanotubes, whereas less ionized surfaces attract fewer nanotubes but were more selective in sorting them by chirality. The electrostatic attraction ultimately served as a competing force to the sorting on the surface, where the stronger the electrostatic attraction the lower efficiency in chirality sorting. Highly protonated surfaces attracted most defective SWNTs and produced unsorted SWNTnts. As the density of surface charges was reduced, interaction between lone pair electrons on the nitrogen atoms on surface and the SWNTs led to chirality sorting. This attraction can be further weakened by restricting access to the amine lone pair electrons with secondary and tertiary amines and resulted in less sorting when these surfaces were used. For this reason, it is clear that the amine, and specifically the lone pair, is crucial in controlling any level of sorting in solution-deposited nanotube networks. Likewise, the hydrogen atom on the amine is not required for adsorption even though it has less steric hindrance than other substituents. Ultimately, tuning the charges on the surface by treating with different pH solutions can serve as a simple method of controlling the density and alignment of the deposited nanotube networks. When utilized in electronic devices, this can serve as a route to tune and optimize device performance.

## EXPERIMENTAL SECTION

**Surface Modification:** Surface modification experiments were performed using both native and thermally grown, 300 nm, oxide on heavily n-doped Si(100) wafers (Silicon Quest). All substrates were held in a Teflon wafer holder and cleaned for 30 min in a piranha bath (3:1 $H_2SO_4/H_2O_2$; caution: highly reactive toward organics). They were subsequently rinsed and sonicated in deionized water for another 30 min. Samples were then dried under $N_2$ and transferred into a dry $N_2$ glovebox for silane modification. SAMs of aminopropyltriethoxysilane (APTES), *N*-methylaminopropyltrimethoxysilane (MAPS), and *N*,*N*-dimethylaminopropyltrimethoxysilane (DMAPS) were purchased from Gelest and distilled prior to use. In the glovebox, the substrates were submerged in a 1% by volume solution of silane in anhydrous toluene for 45 min, 24 h, and 48 h (for APTES, MAPS, and DMAPS, respectively). Following the surface modification, they were rinsed repeatedly with clean anhydrous toluene, sonicated, rinsed again in toluene, then dried under $N_2$, and annealed under vacuum for 20 min at 100 °C before characterization. SAM surface roughness ranged from 0.1 to 0.3 nm.

**Nanotube Solution Preparation:** Details of the nanotube purification and dispersion are provided in a previous publication.[36] Eighty milligrams of arc-dishcarged single-walled nanotubes (AD-SWNTs) obtained from ILJIN Nanotech, grade ASP-100F, and 2 g of sodium dodecyl sulfate (SDS), from J.T. Baker, were mixed with 200 mL of Ultrapure water (0.1 μm filtered, from Invitrogen). The mixture was sonicated in a Cole-Palmer Ultrasonic Processor at 750 W and 100% amplitude for 30 min in an ice−water bath. The sonicated mixture was centrifuged using a Sorvall RC5C Plus centrifuge at 12 500 rpm for 4 h at 4 °C. Approximately 80% of the supernatant was decanted and diluted with anhydrous acetone to dissociate the SDS from the SWNTs. The flocculated SWNTs were collected by centrifugation and rinsed several times with acetone to completely remove SDS. The suspension was filtered through a PTFE membrane (Millipore, 0.45 μm pore size) to collect the nanotubes as a "bucky paper." This was peeled off the membrane, dried under vacuum overnight at 50 °C, and stored in a desiccator. Nanotube solutions were produced by dissolving the bucky paper (by 20 min of ultrasonication at 700 W, 60% amplitude) at a concentration of 10 μg/mL in NMP (*N*-methylpyrrolidone, Omnisolve, spectrophotometry grade).

**pH Modification and CNT Deposition:** Dried substrates were placed in aqueous solutions of HCl or NaOH of varying pH for 20 min; pH was measured using a Fisher Scientific Accumet Excel XL15 pH/mV/temperature meter. Samples were removed, spun-dried for 20 s, then immediately spun-cast with CNT solution. The CNT solution was carefully dropped *via* pipet near the surface in the center of a 2.5 cm × 1.5 cm APTES-modified Si wafer spinning at a speed of 4000 rpm (Headway Research).

**Sample Characterization:** AFM topography images were acquired in the tapping mode regime using a Multimode AFM (Veeco). Images were taken at approximately the same location on each sample (see Supporting Information). Alignment and density analyses were carried out with Image J software (an open source software released by NIH). μ-Raman (LabRam Aramis, Horiba Jobin Yvon) measurements were carried out at 633, 532, and 785 nm (1.96, 2.33, and 1.58 eV, respectively) at 100× magnification with 1 μm spot size and 1200 grating. Excitation power through the filter was 2 mW for the 633 nm line. All data were acquired from automated multipoint (9−12 points) mapping over random regions on the samples, with three spectra accumulated and averaged at each single point. All summarized data were normalized to the 303 $cm^{-1}$ mode in Si, unless stated otherwise.

*Acknowledgment.* This research was supported by the National Science Foundation (NSF) ECCS 0901414, Stanford Global Climate & Energy Program (GCEP), Samsung Advanced Research Institute, and Intel. J.P.O. acknowledges support from the Stanford Graduate Fellowship (SGF). M.C.L. acknowledges support from the Intelligence Community Postdoctoral Fellowship Program. Z.B. acknowledges support from a Sloan Research Fellowship.

*Supporting Information Available:* AFM images comparing alignment at various locations across sample surface. This material is available free of charge *via* the Internet at http://pubs.acs.org.

## REFERENCES AND NOTES

1. Baughman, R. H.; Zakhidov, A. A.; de Heer, W. A. Carbon Nanotubes—The Route Towards Applications. *Science* **2002**, *297*, 787–792.
2. Hu, J. T.; Odom, T. W.; Lieber, C. M. Chemistry and Physics in One Dimension: Synthesis and Properties of Nanowires and Nanotubes. *Acc. Chem. Res.* **1999**, *32*, 435–445.
3. Freitag, M. Carbon Nanotube Electronics and Devices. In *Carbon Nanotubes: Properties and Applications*; O'Connell, M. J., Ed.; CRC Press: Boca Raton, FL, 2006; pp 83−117.
4. Ahn, J.-H.; Kim, H.-S.; Lee, K. J.; Jeon, S.; Kang, S. J.; Sun, Y.; Nuzzo, R. G.; Rogers, J. A. Heterogeneous Three-Dimensional Electronics by Use of Printed Semiconductor Nanomaterials. *Science* **2006**, *314*, 1754–1757.
5. Gruner, G. Carbon Nanotube Films for Transparent and Plastic Electronics. *J. Mater. Chem.* **2006**, *16*, 3533–3539.

6. Hellstrom, S; Lee, H. W.; Bao, Z. Polymer-Assisted Direct Deposition of Uniform Carbon Nanotube Bundle Networks for High Performance Transparent Electrodes. *ACS Nano* **2009**, *3*, 1423–1430.
7. Snow, E. S.; Perkins, F. K.; Robinson, J. A. Chemical Vapor Detection Using Singled-Walled Carbon Nanotubes. *Chem. Soc. Rev.* **2006**, *35*, 790–798.
8. Barone, P. W.; Parker, R. S.; Strano, M. S. *In Vivo* Fluorescence of Glucose Using a Single-Walled Carbon Nanotube Optical Sensor: Design, Fluorophore Properties, Advantages, and Disadvantages. *Anal. Chem.* **2005**, *77*, 7556–7562.
9. Kuzmych, O.; Allen, B. L.; Star, A. Carbon Nanotube Sensors for Exhaled Breath Components. *Nanotechnology* **2007**, *18*, 375502.
10. Star, A.; Han, T.-R.; Joshi, V.; Gabriel, J.-C. P.; Gruner, G. Nanoelectronic Carbon Dioxide Sensors. *Adv. Mater.* **2004**, *16*, 2049–2052.
11. Wang, F.; Gu, H.; Swager, T. M. Carbon Nanotube/Polythiophene Chemiresistive Sensors for Chemical Warfare Agents. *J. Am. Chem. Soc.* **2008**, *130*, 5392–5393.
12. Rowell, M. W.; Topinka, M. A.; McGehee, M. D.; Prall, H.-J.; Dennler, G.; Sariciftci, N. S.; Hu, L.; Gruner, G. Organic Solar Cells with Carbon Nanotube Network Electrodes. *Appl. Phys. Lett.* **2006**, *88*, 233506.
13. Li, C.; Chen, Y.; Wang, Y.; Iqbal, Z.; Chhowalla, M.; Mitra, S. A. Fullerene−Single Wall Carbon Nanotube Complex for Polymer Bulk Heterojunction Photovoltaic Cells. *J. Mater. Chem.* **2007**, *17*, 2406–2411.
14. Arnold, M. S.; Green, A. A.; Hulvat, J. F.; Stupp, S. I.; Hersam, M. C. Sorting Carbon Nanotubes by Electronic Structure Using Density Differentiation. *Nat. Nanotechnol.* **2006**, *1*, 60–65.
15. Kanungo, M.; Lu, H.; Malliaras, G. G.; Blanchet, G. B. Suppression of Metallic Conductivity by Single-Walled Carbon Nanotubes by Cycloaddition Reactions. *Science* **2009**, *323*, 234–237.
16. Strano, M. S.; Dyke, C. A.; Usrey, M. L.; Barone, P. W.; Allen, M. J.; Shan, H.; Kittrell, C.; Hauge, R. H.; Tour, J. M.; Smalley, R. E. Electronic Structure Control of Single-Walled Carbon Nanotube Functionalization. *Science* **2003**, *301*, 1519–1522.
17. Collins, P. G.; Arnold, M. S.; Avouris, P. Engineering Carbon Nanotubes and Nanotube Circuits Using Electrical Breakdown. *Science* **2001**, *292*, 706–709.
18. Yi, W.; Malkovskiy, A.; Chu, Q.; Sokolov, A. P.; Colon, M. L.; Meador, M.; Pang, Y. Wrapping of Single-Walled Carbon Nanotubes by a π-Conjugated Polymer: The Role of Polymer Conformation-Controlled Size Selectivity. *J. Phys. Chem. B* **2008**, *112*, 12263–12269.
19. Krupke, R.; Hennrich, F.; v. Lohneysen, H.; Kappes, M. Separation of Metallic from Semiconducting Single-Walled Carbon Nanotubes. *Science* **2003**, *301*, 344–347.
20. Zheng, M.; Jagota, A.; Semke, E. D.; Diner, B. A.; McLean, R. S.; Lustig, S. R.; Richardson, R. E.; Tassi, N. G. DNA-Assisted Dispersion and Separation of Carbon Nanotubes. *Nat. Mater.* **2003**, *2*, 338–342.
21. Chattophadhyay, D.; Galeska, I.; Papadimitrakopoulos, F. A Route for Bulk Separation of Semiconducting from Metallic Single-Wall Carbon Nanotubes. *J. Am. Chem. Soc.* **2003**, *125*, 3370–3375.
22. Chen, Z.; Du, X.; Du, M.-H.; Rancken, C. D.; Cheng, H.-P.; Rinzler, A. G. Bulk Separative Enrichment in Metallic or Semiconducting Single-Walled Carbon Nanotubes. *Nano Lett.* **2003**, *3*, 1245–1249.
23. Papadimitrakopoulos, F.; Ju, S.-Y. Purity Rolled Up in a Tube. *Science* **2007**, *450*, 486–487.
24. Snow, E. S.; Novak, J. P.; Campbell, P. M.; Park, D. Random Networks of Carbon Nanotubes as an Electronic Material. *Appl. Phys. Lett.* **2003**, *82*, 2145–2147.
25. Cao, Q.; Kim, H.-S.; Pimparkar, N.; Kulkarni, J. P.; Wang, C.; Shim, M.; Roy, K.; Alam, M. A.; Rogers, J. A. Medium-Scale Carbon Nanotube Thin-Film Integrated Circuits on Flexible Plastic Substrates. *Nature* **2008**, *454*, 495–500.
26. Meitl, M. A.; Zhou, Y.; Gaur, A.; Jeon, S.; Usrey, M. L.; Strano, M. S.; Rogers, J. A. Solution Casting and Transfer Printing Single-Walled Carbon Nanotube Films. *Nano Lett.* **2004**, *4*, 1643–1647.
27. Lay, M. D.; Novak, J. P.; Snow, E. S. Simple Route to Large-Scale Ordered Arrays of Liquid-Deposited Carbon Nanotubes. *Nano Lett.* **2004**, *4*, 603–606.
28. Fu, Q.; Liu, J. Integrated Single-Walled Carbon Nanotube/Microfluidic Devices for the Study of the Sensing Mechanism of Nanotube Sensors. *J. Phys. Chem. B* **2005**, *109*, 13406–13408.
29. Lu, M.; Jang, M.-W.; Haugstad, G.; Campbell, S. A.; Cui, T. Well-Aligned and Suspended Single-Walled Carbon Nanotube Film: Directed Self-Assembly, Patterning, and Characterization. *Appl. Phys. Lett* **2009**, *94*, 261903.
30. Zhang, Q.; Vichchulada, P.; Cauble, M. A.; Lay, M. D. Percolation in Networks of Aligned SWNTs Formed with Laminar Flow Deposition. *J. Mater. Sci.* **2009**, *44*, 1206–1211.
31. Choi, K. H.; Bourgoin, J. P.; Auvray, S.; Esteve, D.; Duesberg, G. S.; Roth, S.; Burghard, M. Controlled Deposition of Carbon Nanotubes on a Patterned Substrate. *Surf. Sci.* **2000**, *462*, 195–202.
32. Liu, J.; Casavant, M. J.; Cox, M.; Walters, D. A.; Boul, P.; Lu, W.; Rimberg, A. J.; Smith, K. A.; Colbert, D. T.; Smalley, R. E. Controlled Deposition of Individual Single-Walled Carbon Nanotubes on Chemically Functionalized Templates. *Chem. Phys. Lett.* **1999**, *303*, 125–129.
33. Wang, Y.; Maspoch, D.; Zou, S.; Schatz, G. C.; Smalley, R. E.; Mirkin, C. A. Controlling the Shape, Orientation, and Linkage of Carbon Nanotube Features with Nano Affinity Templates. *Proc. Natl. Acad. Sci. U.S.A.* **2006**, *103*, 2026–2031.
34. Kocabas, C.; Pimparkar, N.; Yesilyurt, O.; Kang, S. J.; Alam, M. A.; Rogers, J. A. Experimental and Theoretical Studies of Transport through Large Scale, Partially Aligned Arrays of Single-Walled Carbon Nanotubes in Thin Film Type Transistors. *Nano Lett.* **2007**, *7*, 1195–1202.
35. Buldum, A.; Lu, J. P. Contact Resistance between Carbon Nanotubes. *Phys. Rev. B* **2001**, *63*, 161403.
36. LeMieux, M. C.; Roberts, M.; Barman, S.; Jin, Y. W.; Kim, J. M.; Bao, Z. Self-Sorted, Aligned Nanotube Networks for Thin-Film Transistors. *Science* **2008**, *321*, 101–104.
37. Gotovac, S.; Honda, H.; Hattori, Y.; Takahashi, K.; Kanoh, H.; Kaneko, K. Effect of Nanoscale Curvature of Single-Walled Carbon Nanotubes on Adsorption of Polycyclic Aromatic Hydrocarbons. *Nano Lett.* **2007**, *7*, 583–587.
38. Star, A.; Han, T.-R.; Gabriel, J.-C. P.; Bradley, K.; Gruner, G. Interaction of Aromatic Compounds with Carbon Nanotubes: Correlation to the Hammett Parameter of the Substituent and Measured Carbon Nanotube FET Response. *Nano Lett.* **2003**, *3*, 1421–1423.
39. Zhao, J.; Lu, J. P. Noncovalent Functionalization of Carbon Nanotubes by Aromatic Organic Molecules. *Adv. Phys. Lett.* **2003**, *82*, 3746–3748.
40. Lu, J.; Lai, L.; Luo, G.; Zhou, J.; Qin, R.; Wang, D.; Wang, L.; Mei, W. N.; Li, G.; Gao, Z.; *et al.* Why Semiconducting Single-Walled Carbon Nanotubes Are Separated from Their Metallic Counterparts. *Small* **2007**, *3*, 1566–1576.
41. Basiuk, E. V.; Basiuk, V. A.; Banuelos, J.-G.; Saniger-Blesa, J.-M.; Pokrovskiy, V. A.; Gromovoy, T. Y.; Mischanchuk, A. V.; Mischanchuk, B. G. Interaction of Oxidized Single-Walled Carbon Nanotubes with Vaporous Aliphatic Amines. *J. Phys. Chem. B* **2002**, *106*, 1588–1597.
42. Kong, J.; Dai, H. Full and Modulated Chemical Gating of Individual Carbon Nanotubes by Organic Amine Compounds. *J. Phys. Chem. B* **2001**, *105*, 2890–2893.
43. Maeda, Y.; Kimura, S.-I.; Kanda, M.; Hirashima, Y.; Hasegawa, T.; Wakahara, T.; Lian, Y.; Nakahodo, T.; Tsuchiya, T.; Akasaka, T.; *et al.* Large Scale Separation of Metallic and Semiconducting Single-Walled Carbon Nanotubes. *J. Am. Chem. Soc.* **2005**, *127*, 10287–10290.

44. Friddle, R. W.; LeMieux, M. C.; Cicero, G.; Artyukhin, A. B.; Tsukruk, V. V.; Grossman, J. C.; Galli, G.; Noy, A. Single Functional Group Interactions with Individual Carbon Nanotubes. *Nat. Nanotechnol.* **2007**, *2*, 692–697.
45. Burgin, T. P.; Lewenstein, J. C.; Werho, D. Investigations into the Mechanism of Adsorption of Carbon Nanotubes onto Aminopropylsiloxane Functionalized Surfaces. *Langmuir* **2005**, *21*, 6596–6602.
46. Usrey, M. L.; Strano, M. S. Adsorption of Single Walled Carbon Nanotubes onto Silicon Oxide Surface Gradients of 3-Aminopropyltri(ethoxysilane) Described by Polymer Adsorption Theory. *Langmuir* **2009**, *25*, 9922−9930.
47. Ausman, K. D.; Piner, R.; Lourie, O.; Ruoff, R. S. Organic Solvent Dispersions of Single-Walled Carbon Nanotubes: Toward Solutions of Pristine Nanotubes. *J. Phys. Chem. B* **2002**, *104*, 8911–8915.
48. Roberts, M. E.; LeMieux, M. C.; Bao, Z. Sorted and Aligned Single-Walled Carbon Nanotube Networks for Transistor-Based Aqueous Chemical Sensors. *ACS Nano* **2009**, *3*, 3287–3293.
49. LeMieux, M. C.; Sok, S.; Roberts, M. E.; Opatkiewicz, J.; Liu, D.; Barman, S. N.; Patil, N.; Mitra, S.; Bao, Z. Solution Assembly of Organized Carbon Nanotube Networks for Thin-Film Transistors. *ACS Nano* **2009**, *3*, 4089–4097.
50. Dresselhaus, M. S.; Dresselhaus, G.; Jorio, A.; Souza Filho, A. G.; Saito, R. Raman Spectroscopy on Isolated Single Wall Carbon Nanotubes. *Carbon* **2002**, *40*, 2043–2061.
51. Jorio, A.; Saito, R.; Hafner, J. H.; Lieber, C. M.; Hunter, M.; McClure, T.; Dresselhaus, G.; Dresselhaus, M. S. Structural (*n*,*m*) Determination of Isolated Single-Wall Carbon Nanotubes by Resonant Raman Scattering. *Phys. Rev. Lett.* **2001**, *86*, 1118–1121.
52. Zhao, J.; Buldum, A.; Han, J.; Lu, J. P. Gas Molecule Adsorption in Carbon Nanotubes and Nanotube Bundles. *Nanotechnology* **2002**, *13*, 195–200.